Kinetic Isotope Effect Characterization of the Transition State for Oxidized Nicotinamide Adenine Dinucleotide Hydrolysis by Pertussis Toxin†

Johannes Scheuring‡ and Vern L. Schramm*

Department of Biochemistry, Albert Einstein College of Medicine, 1300 Morris Park Avenue, Bronx, New York 10461

Received November 18, 1996; Revised Manuscript Received February 4, 1997⊗

ABSTRACT: Pertussis toxin from *Bordatella pertussis* catalyzes the ADP ribosylation of several G-proteins, using NAD^+ as a substrate. In the absence of an acceptor protein, the toxin acts as a NAD^+ glycohydrolase. Pertussis toxin is one of the virulent factors for whooping cough and therefore a target for site-specific inhibitors based on the transition state structure. A family of kinetic isotope effects was determined for the hydrolysis reaction, using NAD^+ labeled with ^3H, ^{14}C, and ^{15}N as substrates. Primary isotope effects were 1.021 ± 0.001 for [1′$_N$-^{14}C]NAD^+ and 1.021 ± 0.004 for [1$_N$-^{15}N]NAD^+, and the double-primary effect of [1′$_N$-^{14}C,1$_N$-^{15}N]NAD^+ was 1.049 ± 0.004. Secondary kinetic isotope effects were 1.207 ± 0.010 for the [1′$_N$-^{3}H]-, 1.144 ± 0.005 for the [2′$_N$-^{3}H]-, 0.989 ± 0.001 for the [4′$_N$-^{3}H]-, and 1.019 ± 0.004 for the [5′$_N$-^{3}H]NAD^+, respectively. Commitment to catalysis was excluded by isotope trapping experiments, and the experimental kinetic isotope effects were independent of pH. The measured isotope effects are therefore intrinsic. The isotope effects are remarkable because they indicate an oxocarbenium-like ribose ring at the transition state but a stiffer than expected vibrational environment for C1′ at the reaction center. On the basis of these isotope effects, a bond order vibrational analysis was performed to locate a transition state structure consistent with the isotope effects. The kinetic isotope effects predict a residual bond order to the nicotinamide leaving group of 0.11, corresponding to a distance of 2.14 Å. Participation of the water nucleophile is weak, consistent either with an S_N1-like transition state with no water interaction or with the water oxygen no closer than 3.5 Å from the reaction center. The positive charge of the ribose oxocarbenium is stabilized by delocalization between the C1′−O4′ and C1′−C2′ bonds. The enzyme contacts restrict the vibrational environment of the reaction coordinate requiring increased bonding force constants for the enzyme-stabilized transition state. NAD^+ analogues with the nicotinamide ribose replaced by an iminoribitol ring, mimicking the flattened ribose ring of the transition state, are expected to be transition state inhibitors.

Pertussis toxin from *Bordatella pertussis* belongs to the group of bacterial ADP-ribosylating toxins which include cholera and diphtheria toxins (Domenighini et al., 1995; Moss & Vaughan, 1988). These enzymes catalyze the transfer of ADP−ribose from NAD^+ [1] to specific acceptor proteins. Pertussis toxin and cholera toxin ADP-ribosylate the α-subunits of several G-proteins, and the substrate of diphtheria toxin is the diphthamide of eukaryotic elongation factor EF2 (Van Ness et al., 1980). The target of ADP ribosylation by pertussis toxin is a cysteine residue, four amino acids from the C terminus of proteins G_i, G_o, and G_t (Katada & Ui, 1982; West et al., 1985). The cholera toxin substrate is arginine residue 201 of G_S and G_T (Van Dop et al., 1984). These G-proteins are involved in the signal transduction between membrane-bound receptor proteins and adenylate cyclase or other proteins regulating pathways in eukaryotic cells (Hepler & Gilman, 1992). ADP ribosylation prevents the normal coupling of the G-protein to its specific receptor molecule and as a consequence interrupts the regulation of the related enzyme cascades. ADP ribosylation of $G_{s\alpha}$ by cholera toxin causes uncontrolled stimulation of the adenylate cyclase; ADP ribosylation of $G_{i\alpha}$ by pertussis toxin prevents the inhibition of adenylate cyclase. In the absence of an acceptor protein, all of these toxins can act as NAD^+ glycohydrolases (Katada et al., 1983), yielding ADP−ribose as the product. However, NAD^+ hydrolysis by pertussis toxin is about 10 times slower than ADP ribosylation of the G-proteins (Locht et al., 1990), and there is no known physiological function of this reaction.

Pertussis toxin is a hexameric protein with a molecular mass of 105 kDa and has, like the other bacterial ADP-ribosylating toxins, an A−B subunit structure (Tamura et al., 1982). The catalytically active subunit is the 26.5 kDa A protomer. The B protomer consists of five subunits and is responsible for receptor recognition and passage of the A protomer through the cell membrane into the cytosol. Prior to catalysis, the enzyme subunit requires activation by reduction of an internal disulfide bridge (Moss et al., 1983). Enzyme kinetic properties of the isolated A protomer and the A−B complex are nearly the same (Katada et al., 1983).

B. pertussis is the causative agent for whooping cough. This and other infectious diseases which are mediated by bacterial toxins remain responsible for a large number of deaths every year, especially in undeveloped countries

† This work was supported by Research Grant AI34342 from the National Institutes of Health.

* Address correspondence to this author. Telephone: (718) 430-2813. Fax: (718) 430-8565. E-mail: vern@aecom.yu.edu.

‡ Current address: Friedrich Schiller Universitaet, Jena, Germany.

⊗ Abstract published in *Advance ACS Abstracts,* April 1, 1997.

[1] Abbreviations: NAD^+, oxidized nicotinamide adenine dinucleotide; NMN, nicotinamide mononucleotide; ADP, adenosine diphosphate; KIE, kinetic isotope effect; DTT, dithiothreitol; BSA, bovine serum albumin. The subscripts $_N$ and $_A$ refer to the NMN and AMP portion of NAD^+, respectively; thus, [1′$_N$-^{14}C]NAD^+ refers to ^{14}C at the 1′ position in the NMN ribosyl portion of NAD^+.

S0006-2960(96)02841-3 CCC: $14.00

(Relman, 1995). Thus, there is a challenge to find new agents for the treatment of these diseases. The toxins are possible targets for development of new site-specific inhibitors. Carbanicotinamide adenine dinucleotide, an analogue of NAD^+, has been synthesized as an inhibitor of ADP-ribosyltransferases like the bacterial toxins (Slama & Simmons, 1989), but tests with cholera toxin showed only weak inhibition of the catalytic activity.

Mimics of the enzyme-stabilized transition states of enzymatic reactions are efficient noncovalent inhibitors (Wolfenden, 1972). An experimental approach to the design of efficient transition state inhibitors of specific enzymatic reactions is to establish details of the enzymatic transition state and to use these data to synthesize transition state analogues (Schramm et al., 1994). Transition state structures for enzyme-catalyzed reactions are not available from examination of stable complexes or by spectroscopic or structural data. Only kinetic methods can be used to predict the structure of enzyme-stabilized transition states. Primary and secondary kinetic isotope effects from specifically labeled substrates, followed by semiempirical calculations and bond energy−bond order vibrational analysis (BEBOVIB; Sims et al., 1977; Horenstein & Schramm, 1993), have been used with some success. Structural data from the enzyme are not required; however, the approach requires that the chemical step of catalysis be one of the rate-limiting steps of the kinetic reaction or be made rate-determining by selecting appropriate experimental conditions. The transition state structures from other *N*-ribohydrolases and transferases, including AMP nucleosidase, nucleoside hydrolase, and purine nucleoside phosphorylase, and cholera toxin have been determined from kinetic isotope effects using these methods (Horenstein et al., 1991; Parkin et al., 1991; Mentch et al., 1987; Kline & Schramm, 1995; Rising & Schramm, 1997). On the basis of the experimentally determined transition state structure, a series of efficient inhibitors has been synthesized for nucleoside hydrolase (Horenstein & Schramm, 1993; Boutellier et al., 1994).

Chemical and enzymatic hydrolysis of NAD^+ has been investigated, and several distinct catalytic mechanisms of this reaction have been proposed [for reviews, see Oppenheimer and Handlon (1992) and Oppenheimer (1994)]. In contrast to the more complex kinetics in the case of the ADP ribosylation reaction, this study of KIE for NAD^+ hydrolysis catalyzed by pertussis toxin A protomer provides a starting model for the more complex reactions which include transfer of the ADP−ribose to the acceptor G-proteins. On the basis of these data, the transition state structure of this enzymatic reaction was explored by kinetic isotope effects and normal mode analysis using the bond energy−bond order vibrational program BEBOVIB (Sims et al., 1977).

MATERIALS AND METHODS

Materials. Pertussis toxin A protomer was purchased from List Biological Laboratories. NADase from *Neurospora crassa* was from Sigma. ^{3}H-, ^{14}C-, and ^{15}N-labeled NAD^+ samples were prepared by published methods (Rising & Schramm, 1994). [8_A-^{14}C]NAD^+ was prepared in a one-step procedure using nicotinamide mononucleotide and [8-^{14}C]ATP (see Figure 1 for atomic numbering).

Initial Rate Kinetics. Samples of 150 μL contained 1.0 μg of pertussis toxin A protomer in 100 mM potassium phosphate (pH 7.5) and 20 mM DTT. NAD^+ concentrations were varied from 5 to 155 μM. Pertussis toxin was incubated for 30 min in the presence of DTT to activate the toxin. The reaction was started by adding the NAD^+ solution, and the mixture was incubated at 37 °C. Samples of 25 μL were taken at time intervals of 20 min, and the product and substrate concentrations were determined by analytical HPLC (RP-18 column; 50 mM ammonium acetate at pH 5.0; detection at 260 nm).

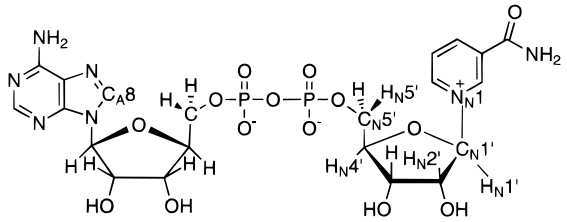

FIGURE 1: Structure of NAD^+ indicating positions in the molecule which were labeled with isotopes for KIE experiments.

Solvent Isotope Effects. Samples containing 3.8 μg/mL pertussis toxin, 100 mM potassium phosphate (pH 7.5), and 20 mM DTT were lyophilized and dissolved in H_2O or D_2O, respectively. The samples were incubated to activate the toxin as described above, and 5×10^4 cpm [8_A-^{14}C]NAD^+ and unlabeled NAD^+ in H_2O or D_2O were added, yielding a final concentration of 210 μM. Samples were taken at 30 min intervals and were analyzed on 1 mL DEAE Sephadex A25 columns, equilibrated with 20 mM ammonium bicarbonate at pH 8.0. NAD^+ was eluted with 6 mL of 150 mM ammonium bicarbonate (pH 8.0) and ADP−ribose with 4 mL of 1.0 M ammonium bicarbonate. Fractions of 2 mL were collected and analyzed by scintillation counting.

Commitment to Catalysis. Samples of 10 μL containing 20 μM activated pertussis toxin and 8×10^4 cpm [8_A-^{14}C]-NAD^+ and unlabeled NAD^+ yielding final concentrations from 30 to 200 μM in 50 mM phosphate (pH 7.5) and 20 mM DTT were incubated at 37 °C for 15 s to form the Michaelis complex. A solution containing 200 μL of 10 mM NAD^+ was added, and the mixture was incubated to allow five catalytic turnovers. The reaction was stopped by the addition of 50 μL of 1 M HCl. Controls for the rate of formation of ADP−ribose used the same amount of enzyme added directly to 200 μL of 10 mM NAD^+ solution, containing 8×10^5 cpm [8_A-^{14}C]NAD^+. The mixture was incubated for the same time periods. To quantitate enzymatic activity during formation of the Michaelis complex, an identical mixture was incubated and samples were retrieved in 20 s intervals. The samples were analyzed on DEAE Sephadex columns as described above.

Measurement of Kinetic Isotope Effects. Identical reaction mixtures containing labeled NAD^+'s were incubated for 20−40% NAD^+ hydrolysis and for 100% hydrolysis. The 100% hydrolysis reaction used NADase from *N. crassa* instead of pertussis toxin. The commercial NADase was purified on Mono Q before use to eliminate phosphatase activity as previously described (Rising & Schramm, 1997). NAD^+ samples containing 10^5 cpm of each of the isotopes in the sensitive and in the remote position (see Table 1) were adjusted with unlabeled NAD^+ to give a final concentration of 100 μM in the reaction samples. The mixture was purified on a Nucleosil RP-18 HPLC column (7.9 × 300 mm) with an eluant of 50 mM ammonium acetate at pH 5.0 and lyophilized. The NAD^+ concentration was established by the ultraviolet absorbance spectrum.

Table 1: Kinetic Isotope Effects of Pertussis Toxin-Catalyzed NAD^+ Hydrolysis

substrates	sensitive isotopic label	KIE
[1′$_N$-^{14}C]- and [4′$_N$-^{3}H]NAD^+	1′-^{14}C, primary[a]	1.021 ± 0.001 (4)[b]
[1$_N$-^{15}N]- and [4′$_N$-^{3}H]-NAD	1-^{15}N, primary[a]	1.021 ± 0.004 (5)
[1$_N$-^{15}N,1′$_N$-^{14}C]- and [4′$_N$-^{3}H]NAD^+	1-^{15}N, 1′-^{14}C, double-primary[a]	1.049 ± 0.004 (4)
[1′$_N$-^{3}H]- and [5′$_N$-^{14}C]NAD^+	1′-^{3}H, α-secondary	1.211 ± 0.010 (3)
[1′$_N$-^{3}H]- and [8$_A$-^{14}C]NAD^+	1′-^{3}H, α-secondary	1.197 ± 0.010 (1)
[2′$_N$-^{3}H]- and [5′$_N$-^{14}C]NAD^+	2′-^{3}H, *β*-secondary	1.144 ± 0.005 (4)
[4′$_N$-^{3}H]- and [5′$_N$-^{14}C]NAD^+	4′-^{3}H, *γ*-secondary	0.989 ± 0.001 (3)
[4′$_N$-^{3}H]- and [8$_A$-^{14}C]NAD^+	4′-^{3}H, *γ*-secondary	0.988 ± 0.003 (1)
[5′$_N$-^{3}H]- and [5′$_N$-^{14}C]NAD^+	5′-^{3}H, *δ*-secondary	1.019 ± 0.004 (2)
[5′$_N$-^{3}H]- and [8$_A$-^{14}C]NAD^+	5′-^{3}H, *δ*-secondary	1.019 ± 0.003 (1)

[a] Observed isotope effects were corrected by the following formula: KIE = (observed KIE)[4′-^{3}H]KIE. [b] The values in parentheses are the number of replicate experiments, each with triplicate or quadruplicate analyses.

Samples for the 20−40% hydrolysis reaction contained 2 μg of pertussis toxin A protomer in 50 mM potassium phosphate (pH 7.5), 20 mM DTT, and 1% BSA in a 300 μL sample. The mixture was incubated for 30 min at room temperature to activate the toxin prior to addition of NAD^+. Reaction mixtures for the complete hydrolysis of NAD^+ contained 0.02 unit of NADase. The reactions were started by the addition of NAD^+, and the samples were incubated for 4 h at 37 °C.

The product ADP−ribose and remaining NAD^+ were separated on Sephadex DEAE columns. Samples of 60 μL were applied to 1 mL columns. Unreacted NAD^+ was eluted with 6 mL of 150 mM ammonium bicarbonate at pH 8.0, and ADP−ribose was eluted with 5 mL of 0.8 M ammonium bicarbonate. Fractions of 0.5 mL were collected.

The ^{3}H/^{14}C ratios of the 20−40% and complete reactions were determined by scintillation counting. The samples of each experiment were counted for at least 10 cycles. The resulting KIEs were calculated using methods described previously (Parkin & Schramm, 1987) and incorporated into a spreadsheet computational program.

Transition State Modeling. The experimental kinetic isotope effects were matched to a transition state structure using the BEBOVIB program (Sims et al., 1977). Coordinates for the reactant state conformation of NAD^+ were taken from the crystal structure of NAD^+ bound to diphtheria toxin (Bell & Eisenberg, 1996; data from the Brookhaven National Laboratory Protein Data Bank, 1TOX). The NMN portion of the molecule was structurally optimized by MOPAC PM3 calculations, freezing two dihedral angles in the ribose ring to maintain the 3′-endo conformation. Coordinates for an oxocarbenium ion transition state are based on the ribonolactone crystal structure (Kinoshita et al., 1981). The carbonyl oxygen was replaced by a hydrogen atom, and the structure was minimized using MOPAC including a positive charge in the molecule. The incoming water nucleophile was modeled as a single oxygen atom. Standard bond lengths and stretching and angle bending force constants for the reactant molecule were taken from Cornell et al. (1995). Bond force constants at the transition states of enzyme-catalyzed reactions are unknown parameters. However, those for bonds more than one bond away from the reaction center were assigned values as above. Those in bonds adjacent to the reaction center were treated as variables since it is conceivable that the crowded environment of an enzymatic catalytic site at the transition state will have a significant effect on stretching or angle bending force constants. The bond lengths, angles, and bond orders were adjusted to fit the experimental KIEs by systematic variation of C1′−N1, C1′−O4′, C1′−C2′, C1′−H1′, C2′−H2′, and C1′−O bond orders (Rising & Schramm, 1997).

Table 2: Substrate Trapping Experiments for Pertussis Toxin

[8$_A$-^{14}C]NAD^+ (μM)[a]	E−NAD^+ (μM)[b]	ADPR formed (μM)[c]	ADPR formed in control (μM)[d]	NAD^+ trapped (μM)[e]
200	17.7	0.42	0.42	0
120	16.3	0.25	0.23	0.02
30	9.3	0.10	0.09	0.01

[a] Total [8$_A$-^{14}C]NAD^+ present to form the pertussis toxin−NAD^+ substrate complex. Pertussis toxin was present at 20 μM in all experiments. [b] Calculated from the apparent dissociation (Michaelis) constant of 24 μM. This is the initial concentration of toxin−labeled NAD^+ complex. [c] Total amount of labeled ADP−ribose formed during the 15 s incubation period and the catalytic turnovers following addition of excess unlabeled NAD^+. [d] Amount of ADP−ribose formed during the 15 s incubation period before addition of excess unlabeled NAD^+. [e] The portion of the original E−NAD^+ complex committed to catalysis.

RESULTS

Initial Rate Kinetics. A K_m value of 24 μM and a k_{cat} of 0.38 min^{-1} were obtained under the conditions of 100 mM potassium phosphate and 20 mM DDT at pH 7.5 and 37 °C. The K_m is in the same range as reported earlier, but the k_{cat} value is smaller than that of 1.1 min^{-1} reported previously (Antoine and Locht, 1994). The difference in buffer conditions used here for the enzyme assays is likely to be the cause of this difference.

Solvent Isotope Effects. A small inverse solvent isotope effect of 0.73 ± 0.09 in terms of initial rates was found for NAD^+ hydrolysis in D_2O. Inverse solvent isotope effects usually indicate the preequilibrium transfer of a deuteron to a site which is involved in catalysis and which prefers deuterium to protium. A similar result has been found for NAD^+ hydrolysis catalyzed by cholera toxin (Rising & Schramm, 1997).

Commitment to Catalysis. In substrate trapping experiments, the toxin was rapidly mixed and incubated with [8$_A$-^{14}C]NAD^+ for 15 s, which resulted in a small fraction of a single turnover. The labeled NAD^+ in the reaction mixture was then diluted 2000−10000-fold with unlabeled NAD^+ solution, and a total of five additional turnovers was allowed. Formation of labeled ADP−ribose following addition of unlabeled NAD^+ was no greater than in control experiments with labeled NAD^+ chemically quenched at the same time (Table 2). In control experiments, the rate of product formation extrapolates in a linear fashion from time zero through 80 s (Figure 2). This result establishes that a catalytically competent complex was formed prior to 15 s,

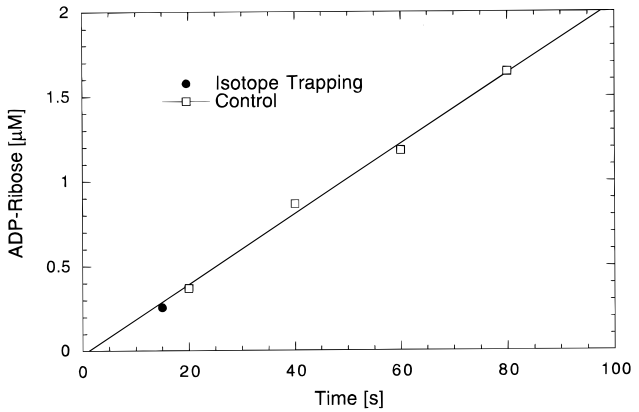

FIGURE 2: Formation of ADP−ribose under pulse experiment conditions [20 μM pertussis toxin and 200 μM [8_A-^{14}C]NAD$^+$ (open symbols)]. The amount of ADP−ribose formed in the trapping experiment is also shown (solid symbol). A 0.1 commitment factor would increase the labeled ADP−ribose formed to a value of 1.6 indicated by the location of the solid symbol labeled Isotope Trapping.

when the isotopic dilution occurred in the trapping experiment. The results establish that hydrolysis of the C1′−N1 bond from the enzyme−NAD$^+$ complex is slow compared to the dissociation of the NAD$^+$−toxin complex. A significant forward commitment to catalysis can be excluded from this result. The results of the pulse−chase trapping experiments are summarized in Table 2.

Kinetic Isotope Effects. Primary and secondary KIEs were measured from the NMN moiety labeled as [$1'_N$-^{14}C]-, [1_N-^{15}N,$5'_N$-^{14}C]-, [1_N-^{15}N,$1'$-^{14}C]-, [$1'_N$-^{3}H]-, [$2'_N$-^{3}H]-, [$4'_N$-^{3}H]-, and [$5'_N$-^{3}H]NAD$^+$. Remote labels were [$5'_N$-^{14}C]- or [8_A-^{14}C]NAD$^+$ for the measurement of ^{3}H KIEs and [$4'_N$-^{3}H]NAD$^+$ for ^{14}C KIEs. The data are summarized in Table 1. The structure of NAD$^+$ indicating the labeled positions is shown in Figure 1.

[$5'_N$-^{14}C]NAD$^+$ was initially used as a remote label for measuring ^{3}H isotope effects. However, the [$5'_N$-^{3}H]NAD$^+$ shows a KIE of 1.019, similar to that reported for cases of other *N*-ribohydrolases (Horenstein et al., 1991; Kline & Schramm, 1993; Rising & Schramm, 1997). This KIE has been interpreted as distortion of the 5′-geometry of ribose during enzymatic catalysis; however, a part of the effect may also result from the ^{14}C label at the 5′-carbon. In order to determine the kinetic isotope effect at the $5'_N$-^{14}C position, [8_A-^{14}C]NAD$^+$ was used as a remote label in separate experiments. The results (Table 1) are the same with ^{14}C at the 8_A and the $5'_N$ positions. Therefore, a significant remote ^{14}C KIE at the 5′-carbon in the NMN moiety does not occur. An advantage of using [8_A-^{14}C]NAD$^+$ as the remote label is the one-step synthesis from NMN and [8_A-^{14}C]ATP compared to the multistep procedure for synthesizing [$5'_N$-^{14}C]-NAD$^+$ from labeled glucose or ribose (Rising & Schramm, 1994).

Primary isotope effects were 1.021 ± 0.001 for [$1'_N$-^{14}C]-NAD$^+$ and 1.021 ± 0.004 for [1_N-^{15}N]NAD$^+$. Both values are relatively small. The KIE from [1_N-^{15}N]NAD$^+$ indicates that there is substantial bond order remaining to the leaving group in the transition state. A maximum ^{15}N KIE of 1.04 could be expected in the case of total dissociation of the nicotinamide leaving group with loss of a full bond order to the nitrogen. The $1'_N$-^{14}C KIE of 1.021 shows that there is little or no interaction between the incoming water nucleophile and the 1′-carbon. The experimental double-primary KIE of 1.049 ± 0.005 from [1_N-^{15}N,$1'_N$-^{14}C]NAD$^+$ is within experimental limits of the calculated value from the product of the primary KIEs which is 1.043 ± 0.009.

Table 3: Kinetic Isotope Effects for [$1'_N$-^{3}H]NAD$^+$ Hydrolysis by Pertussis Toxin as a Function of pH

pH	KIE[a]	k_{cat}, (min^{-1})
6.5	1.220 ± 0.012	0.17 ± 0.02
7.0	1.202 ± 0.008	0.29 ± 0.02
7.5	1.207 ± 0.010	0.38 ± 0.04
8.0	1.216 ± 0.011	0.36 ± 0.04
8.5	1.203 ± 0.015	0.47 ± 0.02
9.0	1.215 ± 0.009	0.39 ± 0.06

[a] KIEs were measured with a mixture of [$1'_N$-^{3}H]NAD$^+$ and [8_A-^{14}C]NAD$^+$ as indicated in Materials and Methods.

Secondary KIEs are 1.207 ± 0.010 in the case of [$1'_N$-^{3}H]NAD$^+$ and 1.144 ± 0.005 for [$2'_N$-^{3}H]NAD$^+$. A large α-secondary KIE is expected if there is increased freedom for the out-of-plane bending motion of the 1′-proton. This motion requires a relatively dissociated transition state and sp^2 hybridization at the 1′-carbon. Large β-secondary isotope effects are the result of hyperconjugation between the 1′- and 2′-carbons, caused by delocalization of the positive charge in the ribose ring. This indicates that the structure of the transition state is oxocarbenium-like.

The [$4'_N$-^{3}H]NAD$^+$ data show a small inverse isotope effect (0.989 ± 0.001). The [$5'_N$-^{3}H]NAD$^+$ value is 1.019 ± 0.002. These isotope effects three and four bonds away from the reaction center and are likely to be due to distortion of the ring system by the enzyme. Similar KIEs in these positions were also observed in the cases of other *N*-ribohydrolases but are not observed in solution solvolysis reactions (Horenstein et al., 1991; Kline & Schramm, 1993; Rising & Schramm, 1997).

The [$1'_N$-^{3}H]NAD$^+$ KIE was measured in the pH range of 6.5−9.0 (Table 3). The results were a constant KIE of 1.21, within the error range. This result is also consistent with the rate-limiting step being *N*-ribosidic bond cleavage which is independent of pH and remains rate-limiting over this pH range.

Transition State Model. Structure of the Reactant. The reactant structure of NAD$^+$ is based on the geometry of the molecule bound to diphtheria toxin (Bell & Eisenberg, 1996). The NMN portion of the molecule was then optimized by MOPAC calculations. The starting point for the transition state structure used an oxocarbenium-like structure of the ribose, based on the structure of ribonolactone (Kinoshita et al., 1981), to obtain a geometry for ribose with sp^2 hybridization at the anomeric 1′-carbon. A truncated structure of the nicotinamide leaving group, representing atoms C2, H2, C3, C5, C6, and H6, was analyzed at a 90° angle to the plane of the O4′−C1′−C2′ bond. Using a truncated structure reduces the number of parameters in the BEBOVIB calculations and does not influence the bonds at the reaction center, provided that all atoms two bonds from the reaction center are included (Sims & Lewis, 1984). The incoming water nucleophile was included as a single O atom, at a 90° angle to the plane of the reaction center.

Bond Order Approach to the Transition State Structure. The transition state structure corresponding to the experimental kinetic isotope effects was first approximated by altering the bond order to the incoming nucleophile (Figure 3). The total bond order at C1′ was held constant by delocalizing the remaining bond order between the C1′−

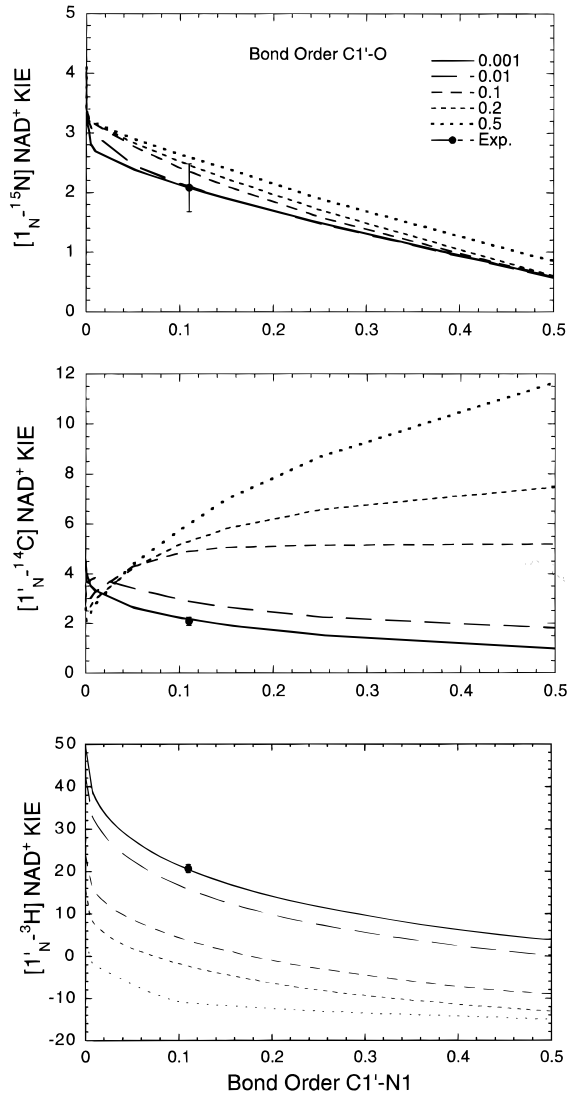

FIGURE 3: Calculated 1_N-^{15}N (top), $1'_N$-^{14}C (middle), and $1'_N$-^{3}H (bottom) kinetic isotope effects for NAD^+ hydrolysis as a function of bond order between C1′ and N1 of the nicotinamide ring at the transition state. The KIEs were calculated for different constant bond orders (C1′−O) to the incoming water nucleophile in a concerted mechanism. The solid circle on each graph is the experimental KIE with the associated error of the measurement. The best fit of all three kinetic isotope effects to the transition state structure occurs at C1′−N1 and C1′−O bond orders of 0.11 and 0.001, respectively.

O4′ and C1′−C2′ bonds. The increased C1′−C2′ bond order was adjusted by a simultaneous decrease in the C2′−H2′ bond order. To match the 1_N-^{15}N KIE, the total bond order at C1′ was delocalized into the surrounding bonds. The α- and β-secondary isotope effects were matched to the appropriate bond orders by adjusting the fraction of the excess bond orders in the C1′−C2′ and C1′−O4′ bonds and by adjusting the bond order of the C1′−H1′ bond. The new parameter set of Cornell et al. (1995) for standard bond lengths and stretching and angle bending force constants was used in the modeling. These values give more detailed information for the specific bonds than the average values used by Sims and Lewis (1984).

These calculations provided a framework for the relationships between bond orders and kinetic isotope effects. The experimental kinetic isotope effects were matched to a transition state with a bond order to the leaving group of 0.11, corresponding to 2.14 Å (Table 4).[2] The incoming water nucleophile had a weak bond order of 0.001 with a distance of 3.5 Å. The best match of transition state structure to the kinetic isotope effects gave a total bond order at the 1′-carbon of 3.62 in the substrate and 3.87 in the transition state when the same bonding force constants were used in the reactant NMN^+ and for the transition state. However, an equally good match was obtained between the experimental kinetic isotope effects and the transition state when the total bond order at C1′ of the reaction center was equal to that of the reactant and either the stretching or angle bending force constants for C1′−O4′ and C1′−C2′ were increased by 10−15% from that of the reactant. The ribose ring has substantial oxocarbenium-like character despite the residual 0.11 bond order to the departing nicotinamide. About 7% of the additional bond order in the ribose ring is delocalized in the C1′−C2′ bond, to account for the H2′ KIE. The positive charge is delocalized over the orbitals of O4′, C1′, and C2′, resulting in nearly a full double bond between C1′ and O4′, and substantial hyperconjugation to C2′. Structures of the truncated substrate and transition state NMN molecules are shown in Figure 4. Transition state structures with a higher bond order to the incipient water nucleophile required large increases of total bond order at the 1′-carbon, resulting in chemically unreasonable structures. Thus, the kinetic isotope effects can best be explained by the oxocarbenium ion transition state with a 0.11 residual bond order to the leaving group and some increase in the bonding force constants at the transition state.

Table 4: Bond Order and Bond Length for NAD^+ Reactant State and Transition State Structures for NAD^+ Hydrolysis by Pertussis Toxin A Protomer

	reactant state		S_N2[a]		S_N1[b]	
bond	bond order	Å	bond order	Å	bond order	Å
C1′−N1	0.84	1.53	0.11	2.14	0.11	2.14
C1′−O4′	1.01	1.41	1.62	1.25	1.59	1.27
C1′−C2′	0.86	1.57	0.92	1.55	0.92	1.55
C1′−H1′	0.90	1.12	0.94	1.11	0.94	1.11
C2′−H2′	0.92	1.11	0.86	1.13	0.86	1.14
C1′−Nu	0	0	0.001	3.50	0	0

[a] The S_N2 transition state involves partial bonding to the attacking water nucleophile (the C1′−Nu bond of Figure 4) in addition to partial bonding to the leaving group (C1′−N1, Figure 4). [b] The S_N1 transition state assumes no bonding to the water nucleophile at the transition state (C1′−Nu bond order = 0).

Participation of the Water Nucleophile. The KIEs were also analyzed for a unimolecular reaction mechanism, in which participation of the nucleophile was omitted (Figure 4). The reaction coordinate of the BEBOVIB file used in these calculations contained only the weak angle bend interaction force constants for the angles of the N1 atom to the ribose ring, with complete loss of the stretching modes. Fitting of the isotope effects to this reaction coordinate resulted in nearly the same transition state structure as determined for the expanded transition state structure (Figures 4 and 5). The incoming water molecule was located at 3.48 Å for the concerned mechanism, indicating a weak or no bonding interaction to H_2O at the transition state.

[2] The model was also calculated using the force constants and standard bond lengths from Sims and Lewis (1984). The resulting transition state structure had a somewhat higher bond order of 0.21 (1.96 Å). Parameters obtained for the ribose ring were nearly the same. However, a difference of 0.2 Å in the distance to the leaving group is beyond the experimental error in kinetic isotope effects. Thus, the more complete parameter set of Cornell et al. (1995) was used.

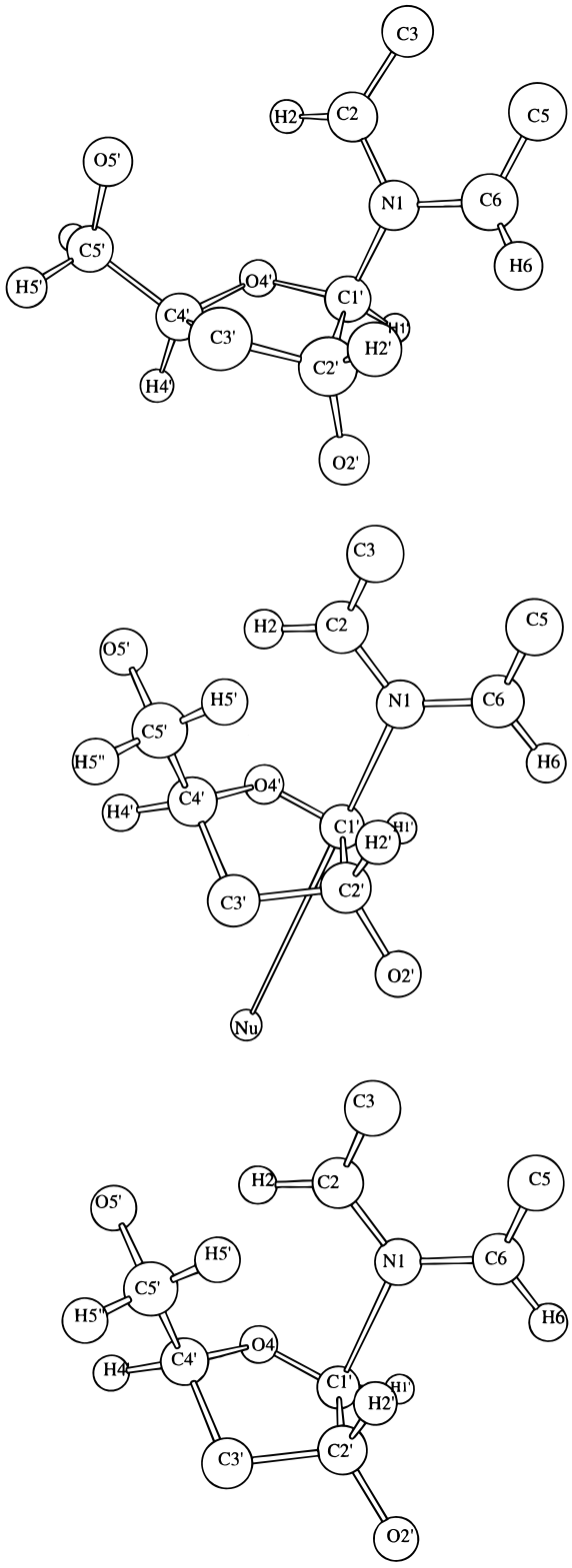

FIGURE 4: Reactant and transition state structures for pertussis toxin NAD^+ hydrolysis. Reactant structure of the NMN portion of NAD^+ used in BEBOVIB calculations (upper). Only atoms used in the BEBOVIB file are shown. The structure is based on the NAD^+ conformation bound to diphtheria toxin (Bell & Eisenberg, 1996). Bond orders and bond lengths are indicated in Table 4. Transition state structure of an S_N2-like mechanism of NAD^+ hydrolysis by pertussis toxin (middle). The incoming water nucleophile (Nu) was calculated as a single oxygen atom. The reaction center in the ribose ring is nearly planar, indicating oxocarbenium ion character. The ribose pucker is 3′-exo. Transition state structure of an S_N1 like mechanism (lower). The extent of C1′−N1 dissociation and structure of the ribose ring at the transition state are nearly the same as that found for the concerned mechanism (Figure 5).

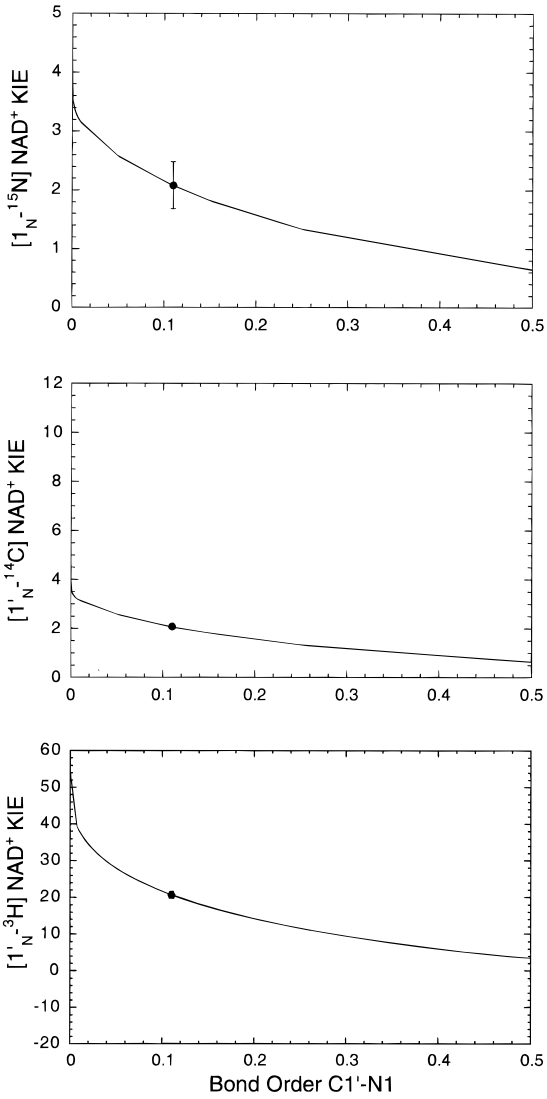

FIGURE 5: Calculated 1_N-^{15}N (top) and $1'_N$-^{14}C (bottom) kinetic isotope effects for a unimolecular mechanism. The analysis was as described in the legend to Figure 3.

The bond order to the leaving group in the unimolecular mechanism is 0.11, the same as in the concerted mechanism. Bond orders in the ribose ring were also similar (Table 4). The total bond order at the 1′-carbon increased from 3.62 for reactant NAD^+ to 3.82 in the transition state with fixed force constants for reactant and transition states. As indicated above, small increases of 10−15% in the force constants adjacent to the reaction center conserved bond order to the reaction center at the transition state. These values are close to those determined in the presence of the water nucleophile.

To determine the transition state structure which gives agreement with the kinetic isotope effects at the $4'_N$-^3H and $5'_N$-^3H positions, the O4′−C4′−C5′ angle was increased to 128°. Calculated and experimental kinetic isotope effects were in agreement using this distortion of the bond geometry.

DISCUSSION

The transition state structure derived from kinetic isotope effects of NAD^+ hydrolysis catalyzed by pertussis toxin has oxocarbenium ion character in the ribose with significant bond order remaining to the nicotinamide ring. There is at most a weak interaction to the incoming water nucleophile. Interpretation of the kinetic isotope effects with and without the incipient water resulted in transition state structures with

only minor differences. Thus, the results indicate a relatively early transition state on a dissociative reaction coordinate. Enzymatic influence on the structure of the transition state is evident from the magnitude of the isotope effects at the reaction center and in remote positions.

Intrinsic Nature of the Kinetic Isotope Effects. Kinetic isotope effects determined for NAD^+ hydrolysis by pertussis toxin are intrinsic. This was demonstrated by the lack of forward commitment to catalysis in the NAD^+ isotope trapping experiment. The reaction rate with a k_{cat} of only 0.38 min^{-1} is slow compared to either the formation or dissociation of the NAD^+−toxin complex. The large α- and β-secondary isotope effects of 1.211 and 1.144 are near those expected for intrinsic KIEs in *N*-ribosyl bond hydrolysis by an oxocarbenium ion transition state. These kinetic isotope effects are similar to those found for the nonenzymatic hydrolysis of NAD^+ (Rising & Schramm, 1997). The double-primary kinetic isotope effect is within the experimental error of the product of the single-primary KIEs. Finally, the independence of the kinetic isotope effect as pH is varied to change the catalytic rate by 2.3-fold indicates that catalysis remains the highest barrier on the reaction coordinate at all of the pH values.

Solvent D_2O Kinetic Isotope Effect. There is a small inverse solvent deuterium isotope effect of 0.73. Inverse solvent isotope effects often indicate a preequilibrium protonation of a group involved in catalysis which prefers deuterium to hydrogen. It has been proposed that His 35 is the enzymatic base involved in activating the nucleophile molecule (Antoine & Locht, 1994). Deprotonation of the water molecule prior to formation of the transition state could give rise to the observed solvent deuterium isotope effect because of the proton fractionation factor for the hydroxide ion (Quinn & Sutton, 1991). However, formation of a hydroxide ion prior to transition state formation would likely increase nucleophilic substitution beyond that observed. A proton transfer as the rate-limiting step would result in a large, normal solvent kinetic isotope effect and can be ruled out. These considerations indicate that only the cleavage of the C1′−N1 bond is rate-limiting in catalysis, but the source of the small inverse solvent isotope effect remains uncertain.

Bond Order to the Nicotinamide Leaving Group. The primary ^{15}N kinetic isotope effect has a relatively small value of 1.021. A maximum KIE approaching 1.04 can be expected for [1_N-^{15}N]NAD^+ in the case of a totally dissociated leaving group. The 1_N-^{15}N KIE is a function of the bond order in the N1−C1′ bond and the bond distribution in the neutral nicotinamide leaving group (Figure 3). It is not sensitive to the delocalization of bond order in the ribose ring.

Bond Order at C1′, the Reaction Coordinate Center. The transition state structure for NAD^+ with a C1′−N1 bond order of 0.110 corresponds to a 2.14 Å bond to the leaving group. This represents an early transition state for NAD^+ hydrolysis, since pH-independent solvolysis gives a significantly more developed oxocarbenium transition state as indicated by a [$1'_N$-^3H]NAD^+ KIE of 1.24 and a bond order of less than 0.05 for this bond (Rising & Schramm, 1997). The $1'_N$-^{14}C KIE is influenced by the bond order to the nucleophile and to the leaving group and is sensitive to the delocalization of the bond order in the ribose ring. The relatively small [$1'_N$-^{14}C]NAD^+ KIE of 1.021 (indicating a restricted vibrational environment) combined with the relatively large [$1'_N$-^3H]NAD^+ kinetic isotope effect (indicating a loose oxocarbenium-like vibrational environment for $1'_N$-^3H) indicates that enzymatic contacts with the transition state stabilize or "stiffen" the bonds to C1′ while permitting free $1'_N$-^3H vibrations. This situation is expressed in normal mode analysis either by increasing total bond order to C1′ at the transition state or by increasing the stretching and/or angle bending force constants to this atom at the transition state. Vacuum ab initio calculations for the C1′ region of this transition state predict a slightly decreased total bond order to C1′ at the transition state. The results therefore suggest that contacts with the catalytic site increase the force constants by 10−15% in the transition state relative to the reactant. Force constant parameters are unavailable for transition states, but calculating ab initio force constants for an sp^2 C═O bond results in a higher force constant than predicted by the linear extrapolation as a function of bond order which is applied for partial bonds formed at the transition state in BEBOVIB calculations (Sims & Lewis, 1984). For these reasons, the total bond order to C1′ was maintained near 3.6 in the transition state (equal to that for reactant) and the match between KIE and transition state structure was obtained by increasing the C1′−O4′ and C1′−C2′ force constants from 4.4 and 4.3 in the reactant to 5.1 and 5.0 in the transition state, respectively (Table 4).

Participation of H_2O at the Transition State. Including weak participation of the attacking water nucleophile in the transition state structure resulted in only minor differences in the bond orders in the ribose ring (Table 4). Bond orders of greater than 0.005 to the oxygen atom of H_2O caused an increase in the predicted $1'_N$-^{14}C and a decrease in the $1'_N$-^3H isotope effects in the normal mode analysis beyond the error limits of the experimental measurements (Table 1). The nearest agreement of isotope effects with transition state structure was obtained at a 0−0.002 bond order to water. The water nucleophile is therefore insignificant in contributing bond order to the transition state.

Oxocarbenium Ion Character of the Transition State. The α- and β-secondary KIEs of 1.21 and 1.14, respectively, establish the oxocarbenium ion-like character of the ribose ring. Expression of an α-secondary ^3H KIE of more than 20% requires a dissociated transition state and a high degree of sp^2 hybridization at the anomeric $1'_N$-carbon atom. Formation of nearly a full double bond between the C1′ and the O4′ and additional hyperconjugation to C2′ stabilizes the positive charge on the ribose ring by delocalization. About 7% of the additional bond order from the loss of the C−N bond is delocalized into the C1′−C2′ bond; the remaining 93% resides in the C1′−O4′ bond. The relatively large H2′ kinetic isotope effect requires this conjugation structure. The increase of bond order in the C1′−C2′ bond causes a decrease of bond order in the C2′−H2′ bond, which is one source of the $2'_N$-^3H KIE. The conformation of the ribose ring also plays a role in the expression of this isotope effect. The 3′-exo conformation of the ribose ring at the transition state results in a H2′−C2′−C1′−N1 dihedral angle near 0°, which permits orbital overlap, hyperconjugation, and the large KIE at H2′. The dihedral angle in the optimized transition state is 3°, near the optimal eclipsed position. Hyperconjugation to the developing empty p orbital on the 1′-carbon atom occurs with this geometry. It is possible that inductive effects by interaction with the toxin could stabilize the developing oxocarbenium ion and influence the bond order of the C2′−H2′ bond (Johnson et al., 1988); however, this interaction is

not required to explain the experimental KIE or the deduced transition state structure.

Remote Kinetic Isotope Effects. The secondary kinetic isotope effects in the remote $4'_N$-^{3}H and $5'_N$-^{3}H positions are not a direct consequence of cleaving the C−N bond. The bond perturbation for kinetic isotope effect measurements rarely extends more than two bonds beyond the site of bond breaking (Sims & Lewis, 1984). However, remote isotope effects are characteristic of several *N*-ribohydrolases but are not observed in the nonenzymatic hydrolysis reactions (Horenstein & Schramm, 1993; Rising & Schramm, 1997). Explanation for this behavior is the enzyme-induced distortion of the ribose during transition state formation on the enzyme.

Relation of the Pertussis Transition State to Other NA-Dases and Proposed Mechanisms. The transition state structure for the hydrolysis of NAD^+ by pertussis toxin is similar to that obtained for cholera toxin (Rising & Schramm, 1997). However, the bond order to the leaving group nicotinamide is lower in the case of the cholera toxin.[3] Thus, both toxins stabilize oxocarbenium ion character at the transition state, but pertussis toxin reaches the transition state earlier in the reaction coordinate.

Previous investigations of the enzymatic and solution hydrolysis of NAD^+ have been recently summarized (Oppenheimer, 1994). A pH-independent mechanism occurs below pH 7 and the pH-dependent mechanism above pH 7 led to the proposal for a diol anion, stabilized transition state for alkaline hydrolysis (Johnson et al., 1988). Several different mechanisms have been reported for enzyme-catalyzed NAD^+ hydrolysis. A covalent enzyme−ADP−ribosyl intermediate has been demonstrated in the case of calf spleen NAD glycohydrolase (Tarnus et al., 1989). The stereochemistry of this enzyme exhibits retention of configuration at the 1′-carbon atom and solvolytic addition from nucleophilic solvents. The ADP-ribosylating bacterial toxins, including pertussis toxin (Scheuring & Schramm, 1995), catalyze inversion of configuration, implying different mechanisms. However, in all of these cases, oxocarbenium-like transition states which lead either to products or to covalent intermediates have been proposed.

Recently, Locht and Antoine (1995) proposed a mechanism for NAD^+ hydrolysis and ADP ribosylation catalyzed by pertussis toxin. On the basis of site-specific mutations and X-ray structural data, they proposed an S_N2 mechanism for both reactions. Glutamate 129 is conserved in all known ADP-ribosylating toxins and is proposed to play a key role in the catalysis by the toxin (Antoine et al., 1993). The crystal structure of NAD^+ bound to diphtheria toxin (Bell & Eisenberg, 1996) showed that the equivalent residue, Glu 123, is in proximity to the reaction center with possible contacts to the $2'_N$-OH, the $1'_N$-carbon, and the nicotinamide ring, all of which are at a distance of about 4 Å. The mechanism proposes glutamate deprotonating the $2'_N$-OH group followed by formation of a diol anion and attack of the water nucleophile. His 35 has been proposed to play a role in the activation of the water or cysteine nucleophile.

The kinetic isotope effects reported here are inconsistent with an S_N2 mechanism or 2′-OH ionization for pertussis toxin. Alkaline solvolysis of NAD^+ is thought to involve ribose hydroxyl ionization and gives a solvent isotope effect of 2.7 (Johnson et al., 1988; Oppenheimer, 1994). The inverse value of 0.73 with pertussis toxin argues against proton transfers at the transition state. Pertussis toxin catalyzes the ADP ribosylation of a synthetic peptide by inversion of configuration at the 1′-carbon (Scheuring & Schramm, 1995), in agreement with a concerted mechanism. The substrate kinetic isotope effects demonstrate that the interaction to the incoming nucleophile in the case of NAD^+ hydrolysis is negligible, at least 3.5 Å between the ribose 1′-carbon and the water molecule. However, at the transition state, bond order of approximately 0.11 remains to the leaving group. The transition state structure is characteristic of an S_N1 reaction coordinate for NAD^+ hydrolysis, where the transition state is achieved early, with partial bond order remaining to the leaving group, before significant nucleophilic attack occurs.

Implications for the ADP Ribosylation Reaction of Pertussis Toxin. NAD^+ hydrolysis by pertussis toxin is only observed in vitro. Water molecules are likely to be present in the unoccupied binding site for the acceptor G-protein. In the presence of an acceptor for ADP ribosylation, this site is occupied with the specific cysteine residue located near the ribose of NAD^+. Pertussis toxin does not catalyze the ADP ribosylation of small thiol molecules like dithiothreitol or free cysteine (McDonald et al., 1992). There is also no evidence for methanolysis catalyzed by the toxin. Only peptides of at least 10 amino acids, corresponding to the C terminus of one of the G-proteins, are suitable substrates (Graf et al., 1992). This implies that the interactions which bind the ADP−ribose acceptor to the toxin involve residues in addition to the cysteine. Successful ADP ribosylation occurs only if the acceptor is poised at the correct position when the active center generates the ADP−ribosyl oxocarbenium ion from NAD^+. Direct access of bulk solvent molecules to the reaction center can be excluded on the lack of reactivity with methanol. Compared to ADP ribosylation, hydrolysis is a relatively slow reaction with a k_{cat} between 0.38 min^{-1} (this study) and 1.1 min^{-1} (Antoine & Locht, 1994). A k_{cat} value of 10 min^{-1} for ADP ribosylation of the G-protein transducin (G_T) has been reported (Cortina et al., 1991). In the hydrolysis reaction, a water molecule bound in the acceptor binding site and activated, possibly by His 35, attacks the oxocarbenium ion developed at the transition state in the catalytic site. Methanol is apparently inefficient at binding to this site.

The transition state of NAD^+ hydrolysis catalyzed by pertussis toxin is similar to those of other enzymatic *N*-ribohydrolase reactions. An oxocarbenium-like transition state is characteristic of all of these enzymes, but with different degrees of C−N bond order and water participation at the transition state. Compounds like phenyliminoribitol and phenylriboamidrazone and derivatives have been synthesized as transition state analogues for these reactions, on the basis of their similarity in geometry and electrostatic potential surface, and were found to be potent inhibitors, with K_i values as low as 2 nM (Horenstein & Schramm, 1993; Boutellier et al., 1994; Parkin & Schramm, 1995). Using some features of these compounds may be a productive starting point for development of inhibitors against pertussis toxin. However, preliminary studies of these nucleoside analogues with pertussis toxin showed no inhibition. The crystal structure of NAD^+ bound to diphtheria toxin (Bell & Eisenberg, 1996) shows multiple interactions between the toxin and the AMP moiety of the molecule. Assuming a similar binding mode to pertussis toxin, a pyrophosphate diester link to an AMP moiety from these inhibitors may be a successful way to develop potent inhibitors.

ACKNOWLEDGMENT

The authors thank Dr. Paul J. Berti for writing the program which calculates the isotope effects from the multichannel scintillation counter data, for helpful discussions of ab initio structures of models of oxocarbenium ions, and for his critical reading.

REFERENCES

Antoine, R., & Locht, C. (1994) *J. Biol. Chem. 269*, 6450−6457.
Antoine, R., Tallett, A., Van Heyningen, S., & Locht, C. (1993) *J. Biol. Chem. 268*, 24149−24155.
Bell, C. E., & Eisenberg, D. (1996) *Biochemistry 35*, 1137−1149.
Boutellier, M., Horenstein, B. A., Semenyaka, A., Schramm, V. L., & Ganem, B. (1994) *Biochemistry 33*, 3994−4000.
Cornell, W. D., Ciepak, P., Bayly, C. I., Gould, I. R., Merz, K. M., Jr., Ferguson, D. M., Spellmeyer, D. C., Fox, T., Caldwell, J. W., & Kollman, P. A. (1995) *J. Am. Chem. Soc. 117*, 5179−5197.
Cortina, G., Krueger, K. M., & Barbieri, J. T. (1991) *J. Biol. Chem. 266*, 23810−23814.
Domenighini, M., Pizza, M., & Rappuoli, R (1995) Bacterial Toxins and Virulence Factors in Disease, in *Handbook of Natural Toxins* (Moss, J., Vaughan, M., Iglenski, B., Vaughan, M., & Tu, A., Eds.) Vol. 8, pp 59−80, Dekker, New York.
Gierschik, P. (1992) in *Current Topics in Microbiology and Immunology*, Vol. 175, pp 69−96, Springer, Berlin and Heidelberg.
Graf, R., Codina, J., & Birnbaumer, L. (1992) *Mol. Pharmacol. 42*, 760−764.
Hepler, J. R., & Gilman, A. G. (1992) *Trends Biochem. Sci. 17*, 383.
Horenstein, B. A., & Schramm, V. L. (1993) *Biochemistry 32*, 9917−9925.
Horenstein, B. A., Parkin, D. W., Estupinan, B., & Schramm, V. L. (1991) *Biochemistry 30*, 10788−10795.
Johnson, R. W., Marschner, T. M., & Oppenheimer, N. J. (1988) *J. Am. Chem. Soc. 110*, 2257−2263.
Katada, T., & Ui, M. (1982) *Proc. Natl. Acad. Sci. U.S.A. 74*, 3129−3133.
Katada, T., Tamura, M., & Ui, M. (1983) *Arch. Biochem. Biophys. 24*, 290−298.
Kinoshita, Y., Ruble, J. R., & Jeffrey, G. A. (1981) *Carbohydr. Res. 92*, 1−7.

[3] In cholera toxin, the hydrolytic transition state for NAD^+ was determined to have a C1′−N1 bond order of 0.11, using the force constants of Sims and Lewis (1984). When recalculated with the improved parameter set of Cornell et al. (1995), this corresponds to a bond order of approximately 0.05. Thus, the C1′−N1 bond at the transition state of cholera toxin has only about half of the transition state bond order found for pertussis toxin.

Kline, P. C., & Schramm, V. L. (1993) *Biochemistry 32*, 13212−13219.
Locht, C., & Antoine, R. (1995) *Biochimie 77*, 333−340.
Locht, C., Labet, Y., Feron, C., Cieplak, W., & Keith, J. M. (1990) *J. Biol. Chem. 265*, 4552−4559.
McDonald, L., Wainschel, L. A., Oppenheimer, N. J., & Moss, J. (1992) *Biochemistry 31*, 11881−11889.
Melander, L., & Saunders, W. H., Jr. (1980) in *Reaction Rates of Isotopic Molecules*, pp 225−227, John Wiley & Sons, New York.
Mentch, F., Parkin, D. W., & Schramm, V. L. (1987) *Biochemistry 26*, 921−930.
Moss, J., & Vaughan, M. (1977) *J. Biol. Chem. 252*, 2455−2457.
Moss, J., & Vaughan, M. (1988) *Adv. Enzymol. 61*, 303−379.
Moss, J., Stanley, S. J., Burns, D. L., Hsia, J. A., Yost, D. A., Myers, G. A., & Hewlett, E. L. (1983) *J. Biol. Chem. 258*, 11879−11882.
Oppenheimer, N. J. (1994) *Mol. Cell. Biochem. 138*, 245−251.
Oppenheimer, N. J., & Handlon, A. L. (1992) in *The Enzymes*, Vol. XX, Academic Press, San Diego.
Parkin, D. W., & Schramm, V. L. (1987) *Biochemistry 26*, 913−920.
Parkin, D. W., & Schramm, V. L. (1995) *Biochemistry 34*, 13961−13966.
Parkin, D. W., Mentch, F., Banks, G. A., Horenstein, B. A., & Schramm, V. L. (1991) *Biochemistry 30*, 4586−4594.
Quinn, D. M., & Sutton, L. D. (1991) in *Enzyme Mechanism from Isotope Effects* (Cook, P. F., Ed.) pp 73−126, CRC Press, Boca Raton, FL.
Relman, D. (1995) Bacterial Toxins and Virulence Factors in Disease, in *Handbook of Natural Toxins* (Moss, J., Vaughan, M., Iglenski, B., & Tu, M., Eds.) Vol. 8, pp 367−405, Dekker, New York.
Rising, K., & Schramm, V. L. (1994) *J. Am. Chem. Soc. 116*, 6531−6536.
Rising, K., & Schramm, V. L. (1997) *J. Am. Chem. Soc. 119*, 27−37.
Scheuring, J., & Schramm, V. L. (1995) *J. Am. Chem. Soc. 117*, 12653−12654.
Schramm, V. L., Horenstein, B. A., & Kline, P. C. (1994) *J. Biol. Chem. 269*, 18259−18262.
Sims, L. B., & Lewis, D. E. (1984) *Isot. Org. Chem. 8*, 161−249.
Sims, L. B., Burton, G. W., & Lewis, D. E. (1977) *QCPE 337*.
Slama, J. T., & Simmons, A. M. (1989) *Biochemistry 28*, 7688−7694.
Tamura, M., Nagimori, K., Murai, S., Yajima, M., Ito, K., Katada, T., Ui, M., & Ishii, S. (1982) *Biochemistry 21*, 5516−5522.
Tarnus, C., Muller, H. M., & Schuber, F. (1988) *Bioorg. Chem. 16*, 38−51.
Van Ness, B. G., Howard, J. B., & Bodley, J. W. (1980) *J. Biol. Chem. 255*, 10710−10716.
West, R. E., Jr., Moss, J., Vaughan, M., Liu, T., & Liu, T.-Y. (1985) *J. Biol. Chem. 260*, 14428−14430.
Wolfenden, R. (1972) *Acc. Chem. Res. 5*, 10−18.

BI962841H